


# Evaluation of an early flood warning system in Bamako (Mali): Lessons learned from the flood of May 2019

Nanée Chahinian<sup>1</sup>  | Matias Alcoba<sup>2</sup> | Ndji dit Jacques Dembélé<sup>3</sup> | Frédéric Cazenave<sup>2</sup> | Christophe Bouvier<sup>1</sup>

<sup>1</sup>HSM (Univ Montpellier, CNRS, IRD), Montpellier, France

<sup>2</sup>IGE (Univ. Grenoble Alpes, Grenoble INP, CNRS, IRD), Grenoble, France

<sup>3</sup>Université des Sciences Sociales et de Gestion de Bamako, Bamako, Mali

## Correspondence

Nanée Chahinian, UMR HydroSciences Montpellier, Université de Montpellier CC 57, 163 rue Auguste Broussonnet, 34090 Montpellier, France.

Email: [nanee.chahinian@ird.fr](mailto:nanee.chahinian@ird.fr)

## Funding information

Korean Green Growth Fund, Grant/Award Number: 1212152

## Abstract

Devastating floods have plagued many West African cities in the past decades. In an attempt to reduce flood damage in Bamako (Mali), an early warning system (EWS) demonstrator (Raincell App) was developed for flash floods. On 16 May 2019, while the demonstrator was partially operational, an intense rainfall event led to devastating floods. We carried out an experience feedback on this flood event by comparing EWS simulations to the results of a field survey. Given the synoptic situation and the rapid development pattern of the storm, none of the global forecasting systems were able to foresee its occurrence and magnitude. The hydrological model developed as part of the demonstrator correctly identified most of the locations where overbank flow occurred. In the absence of data, the predicted discharge and volume values could not be validated. However, they are realistic based on the water levels reported in the Post-Disaster Needs Assessment report. It would be advisable to couple it to a two-dimensional hydraulic model and add discharge and water level monitoring to the already existing rainfall surveillance scheme to further improve the system's performance. Increasing the local population's awareness of the dangers of clogged waterways is also mandatory.

## KEYWORDS

early warning systems, experience feedback (EF), flash flood, forecasting and warning, hydrological modelling, pluvial flooding, rainfall estimation, urban hydrology, West Africa

## 1 | INTRODUCTION

African cities are prone to recurring flooding due to the conjunction of tropical or equatorial rainfall, insufficient and often even non-existing or clogged drainage networks (Bouvier et al., 2018; Egbinola et al., 2017; Mahmood et al., 2017), and urban growth. Unfortunately, the trend is increasing (Di Baldassarre et al., 2010). In the past decades, devastating floods have occurred in West

Africa, namely, in Niamey (2004), Ouagadougou (2009), Dakar (2012) and Bamako (2013–2019) (Descroix, 2018). The 2009 flood in Ouagadougou is reported to have caused eight deaths and destroyed more than 250 houses (Tazen et al., 2018), while the 2019 flood in Bamako caused 16 deaths and destroyed 124 houses (Republic of Mali, 2019).

Early warning systems (EWS) are cited as one of the components of an integrated flash flood management

This is an open access article under the terms of the [Creative Commons Attribution](https://creativecommons.org/licenses/by/4.0/) License, which permits use, distribution and reproduction in any medium, provided the original work is properly cited.

© 2022 The Authors. *Journal of Flood Risk Management* published by Chartered Institution of Water and Environmental Management and John Wiley & Sons Ltd.

scheme in African cities (Horn & Elagib, 2018). They are usually composed of four inter-related elements: (1) assessments and knowledge of flood risks in the area, (2) local hazard monitoring (forecasts) and warning service, (3) flood risk dissemination and communication service and (4) community response capabilities (UN-ISDR, 2013). These systems are known to be cost effective at local, national, continental, and global scales (Alfieri et al., 2019; Pappenberger et al., 2015; Verkade & Werner, 2011). However, according to a survey carried out in 2014, out of the 17 countries in West Africa, only one, Ghana, had an EWS that was considered moderately effective in reducing humanitarian impacts (Lumbroso, 2018; Lumbroso et al., 2014).

In the past decades, EWS development has progressed greatly, and many operational systems have been developed (see reviews in Emerton et al., 2016; Hally et al., 2015; Perera et al., 2019). Nevertheless, despite the technical advances in real-time rainfall and water level monitoring, the detection of flash floods is still considered a major challenge (Perera et al., 2020). This can mainly be explained by the sudden nature of flash floods and the fast hydrological response times they induce. Flash flood EWS systems can be divided into two broad categories. Both use rainfall data either through predictions, nowcasting or monitoring. Their difference lies in the systems and models used to simulate water levels and inundation zones. Data-driven systems rely on historical flood databases and use statistical and stochastic models (Llort et al., 2014; Yang et al., 2015) and, more recently, machine learning techniques (Garcia et al., 2016; Lee et al., 2020), to predict water levels. The second family of systems uses hydrological (Bouvier et al., 2018; Javelle et al., 2016) or hydraulic models (Chitwatkulsiri et al., 2021; Hofmann & Schüttrumpf, 2019) for water level, discharge, or inundation plane prediction. Sometimes, the two approaches may be combined (Lee et al., 2020).

However, most of the systems using hydraulic models have only been applied to small catchments with areas smaller than 100 km<sup>2</sup>. Indeed, Chitwatkulsiri et al. (2021) used MIKE URBAN on the Sumkevit area of Bangkok (24 km<sup>2</sup>), Lee et al. (2020) used the Storm Water Management Model (SWMM) and the Hydrologic Engineering Center-River Analysis System (HEC-RAS) on the Dorim catchment (42.5 km<sup>2</sup>) in the Seoul Metropolitan area, while Hofmann and Schüttrumpf (2019) used SWMM and TUFLOW on a 26 km<sup>2</sup> zone located in the city of Aachen (Germany). Yang et al. (2015) considered these systems to be too slow and less suitable for emergency response. In addition, they must rely on adequate data on local topography and initial conditions, and this constitutes a serious limitation when working in data scarce

settings. Hence, alternative solutions need to be found through a compromise between data availability, calculation time, and accurate predictions.

In an effort to improve flood protection in the city of Bamako (Mali), an EWS demonstrator (“Raincell App”) was developed by a team of scientists from the French National Research Institute for Sustainable Development in partnership with the Civil Protection of Mali (DGPC), MALI-METEO, and the National Hydraulic Directorate (DNH) of Mali. MALI-METEO is responsible for rainfall measurements and weather forecasting throughout the country, while DNH is in charge of water flow and level monitoring. When MALI-METEO identifies a storm system that is likely to cause flooding in a given locality or when DNH’s observations indicate that water levels are on the rise and have exceeded pre-set thresholds, they notify the Civil Protection by telephone. These procedures rely heavily on human operators and work in a parallel mode, that is, the rainfall predictions are not converted into flow or flood maps (Seidou & Diabété, 2019).

On 16 May 2019, while the demonstrator was partially operational, an intense rainfall event led to devastating floods in Bamako. This work aims to evaluate the performance of EWSs in flash flood forecasting at the scale of African cities through an ex-post evaluation on the city of Bamako and the 16 May event. The originality lies in the use of a fully gridded model to simulate a very intense event on a large urban area. The paper is structured as follows: Section 1 presents the study zone, the EWS, and the methodology followed for the field survey. Section 2 describes the modelling and field survey results for the 16 May 2019 flood event. The advantages, limitations, and possible improvements of the EWS are highlighted in the discussion and conclusions section (Section 3).

## 2 | MATERIALS AND METHODS

### 2.1 | The Bamako urban catchment

Bamako, the capital city of the Republic of Mali, is located at 12°38′21″ N and 8°0′10″ W. It straddles the Niger River, which crosses the city in an East–West direction. Fluvial erosional landforms and alluvial deposits dominate the local landscape of the city. Bamako is a depression surrounded by hills made of different materials: palaeozoic sandstones on the left bank that connect to the Niger River valley through cliffs of about 35°–45° and quaternary lacustrine and fluvial hills made of silts and fluvial sands. Elevations in the city range between 500 and 300 m from the river channel. Numerous intermittent rivers flowing down the hills drain the city and

provoke floods during extreme rainfall events. The 10 most important ones are Woyowayanko, Diafaranako, Balassago, Bankoni, Molobalini, Sotuba, Mafiladjida on the left bank and Niamakoro, Magnambougou, Missabougou on the right bank. Their main characteristics are presented in Table 1.

The city has a total area of 267 km<sup>2</sup> and is subdivided into six communes, each headed by an elected mayor. According to a household survey carried out in 2018, the city had 2,419,609 inhabitants and represented 12.6% of Mali's urban population (Republic of Mali, 2019). Over the 2000–2015 period, the population of the Bamako District has more than doubled, and experts anticipate the pressure on the city to grow in the future (Mukim, 2018).

### 2.1.1 | The Bamako experimental catchments

As part of the Raincell App project, three experimental urban catchments were equipped with stream gauges and rain gauges (Figure 1). Their main characteristics are presented in Table 2. The three catchments have areas ranging from 3.4 to 43.2 km<sup>2</sup> and correspond to various levels and types of urban development. Cité Niger and Faladié have similar characteristics. They are smaller and more urbanised than Bolibana, which is the largest and least urbanised of the three and has a more spread-out urban fabric. All three are drained by a network of drainage ditches (Figure 1). Rainfall and discharge monitoring was carried out during the 2017 and 2018 rainy seasons, that is, from May to October. Water levels measured by the stream gauges were converted into discharge by means of a rating curve established for the three locations. In order to avoid loss of equipment, the measuring devices were pulled out during the dry season. On 16 May 2019, only the rainfall gauges were operating, and water level measurements were resumed a few days after the event.

**TABLE 1** Main characteristics of Bamako's watercourses

	Catchment name	Area (km <sup>2</sup> )	Maximum stream length (km)
Left bank	Woyowayanko	159	20
	Diafaranako	40	16
	Balassago	14	08
	Bankoni	51	15
	Molobalini	12	09
	Sotuba	08	04
	Mafiladjida	91	25
Right bank	Niamakoro	42	11
	Magnambougou	08	05
	Missabougou	159	25

## 2.2 | The EWS chain

The Raincell App demonstrator produces rainfall and runoff accumulation maps at the scale of an entire city at 15-min time steps from the beginning of a rainfall event until its end. The system also produces flood warning maps at the same time step.

The chain is fed with rainfall data measured by a rain gauge network and tele-transmitted in real-time through SMS messages every 5 min. It is then transformed into rainfall accumulation data at 5- and 15-min time steps. The 5-min data is used to visualise rainfall hyetograms at five locations in the city, while the 15-min data is used to feed the rainfall-runoff model and create discharge, velocity, and flow height maps, that is, the data displayed on the flood warning maps.

The maps are displayed through a web browser on a PC, mobile phone, or tablet using GeoServer and an Open Street Map (OSM) background. Four menus allow the user to select the information to be displayed, that is, accumulated rainfall over the last 15 min and since the beginning of the rainfall event, discharge throughout the drainage network, and 'flooding severity'.

The server is composed of a Linux CentOS 7 workstation. Its capacity has been scaled to allow fast runs of the hydrological modelling and rainfall data managing programmes (under 15 min). The workstation includes an Intel Xeon E3-1275V5 quad-core/8 threads processor at 3.6 GHz (or 4 GHz in turboboost mode) coupled to 8 Mb of cache memory and 32 Gb of RAM. The forecasting chains have been coded in Javascript (geoserver), Python, R and BASH.

## 2.3 | The rainfall-runoff model

The rainfall-runoff model is part of the ATHYS (ATelier de Modélisation Hydrologique Spatialisée, <http://www.athys.org>).

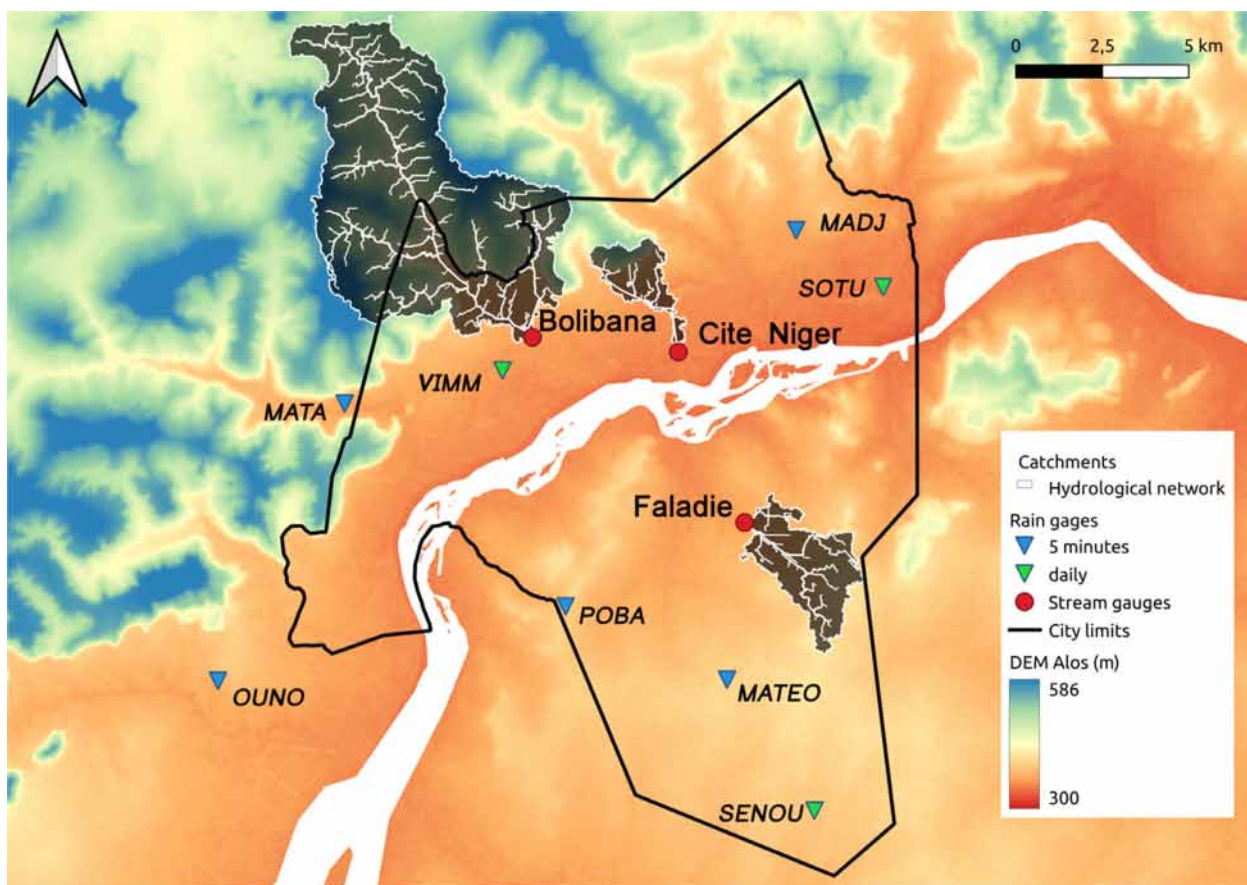


FIGURE 1 The study zone and experimental setting.

Catchment name	Area (km <sup>2</sup> )	% urban cover	Slope (m/m)
Bolibana	43.2	33	0.010
Cité Niger	3.4	56	0.051
Faladié	7.4	59	0.054

TABLE 2 Main characteristics of the experimental catchments

[athys-soft.org/](http://athys-soft.org/)) modelling platform (Bouvier et al., 2018; Bouvier & Delclaux, 1996; Lhomme et al., 2004).

The catchment is divided into  $10 \times 10$  m elementary square cells. In order to determine the drainage directions, the building blocks have been 'burnt' into a digital elevation model (DEM). The elevations of the cells corresponding to the building blocks, that is, groups of traditional houses surrounded by a wall, have been raised by 25 m to compensate for the natural slope between a cell and its neighbours. The drainage directions of the stormwater network have also been modified along each segment from its highest end to the lowest one. The drainage directions have been automatically forced to follow these changes using ATHYS's in-built procedure, as described by Bouvier et al. (2018).

The 'Advanced Land Observing Satellite - Phased Array type L-band Synthetic Aperture Radar' (ALOS

PALSAR, <https://asf.alaska.edu/data-sets/sar-data-sets/alos-palsar/>) DEM has been used in this study. It has been projected in the Universal Transverse Mercator system and re-sampled using the nearest neighbour method at 10 m. The DEM's original spatial resolution is of 12 m. We used 10 m as a compromise between adequate representation of urban features and low calculation times. The accuracy on the elevation is 1 m. Rainfall at a 15-min time step is interpolated on each cell using Thiessen's polygons. The interpolation of rainfall is a delicate and essential task to predict pluvial flooding (Foehn et al., 2018) as the uncertainty and biases it may generate propagate through the hydrological model. We carried out sensitivity tests (not presented herein) comparing Thiessen's method to kriging and found that the sensitivity to interpolation was of second order compared to the hydrological model's calibration sensitivity. Note that the

model can also process other rainfall fields when available (radar or microwave link fields).

On each 10 m cell, a reservoir model using a runoff coefficient is used to calculate the runoff (Figure 2a). The runoff coefficient is constant in time as on urban catchments, this assumption is made when working on whole catchments. It is not necessarily justified when working at smaller scales. However, this choice is made for the sake of simplicity, and the assumption is supported by our data since a linear relationship can be observed when comparing the measured rainfall to the measured runoff values, even for high rainfall values ( $R^2 = 0.81$  for Fala-diyé; 0.76 for Cité Niger, and 0.65 for Bolibana).

$$P_n(t) = RC \times P_b(t) \text{ if } P_{cum}(t) > P_i; \text{ else } P_n(t) = 0. \quad (1)$$

where  $P_n(t)$  is net rainfall rate at time  $t$  [L/T],  $P_b(t)$  is total rainfall rate at time  $t$  [L/T],  $P_{cum}(t)$  is cumulated total rainfall at time  $t$  [L],  $P_i$  is ponding loss [L] and RC is runoff coefficient [L/L].

$P_i$  and RC are the parameters that need to be determined or calibrated. The model uses two routing functions:

The lag and route for natural or peri-urban subcatchments. This transfer function is selected to shorten the computation time in areas that are not subjected to flooding hazards. Each cell  $m$  produces an elementary hydrograph:

$$Q_m(t) = A \times \int_{t_0}^{t-T_m} \frac{P_n(\tau)}{K_m} \times \exp\left(-\frac{t-T_m-\tau}{K_m}\right) d\tau, \quad (2)$$

$$T_m = \sum_k \frac{V_0}{l_k}, \quad (3)$$

$$K_m = K_0 \times T_m, \quad (4)$$

where  $A$  is cell area [ $L^2$ ],  $T_m$  is routing time [T],  $K_m$  is lag time [T],  $l_k$  is length of each cell 'k' of the trajectory between the cell 'm' and the outlet [L].

For horizontal or vertical flow directions, this corresponds to the length of the cell. For diagonal flow directions, this corresponds to the length of the cell times the diagonal (Figure 2b).

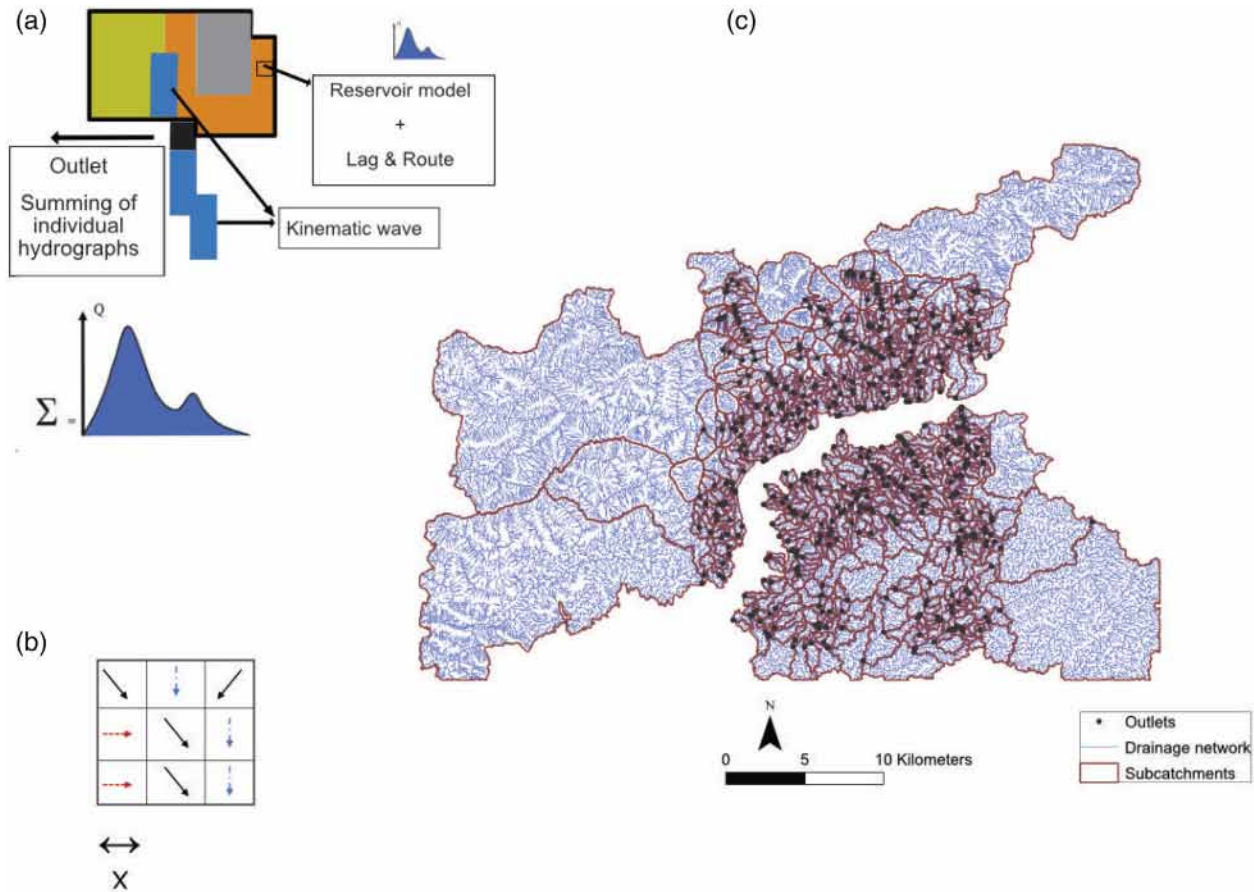


FIGURE 2 Model setting (a), example of flow directions (b) and map of the hydrological units (c) of the Bamako catchment. The dotted arrows correspond to vertical (blue) and horizontal (red) flows. The full lines correspond to diagonal flow. In the first two cases  $l_k = x$ . In the third case  $l_k = x\sqrt{2}$ .

$V_0$ , is flow velocity on each cell [L/T],  $K_0$  is linearity coefficient between  $K_m$  and  $T_m$ .

$V_0$  and  $K_0$  depend on slope and hydraulic resistance. In this work,  $K_0$  has been empirically set to  $K_0 = 0.7$ , as previously done in similar African settings by Bouvier et al. (2018). Then  $V_0$  was calibrated using the rainfall-runoff data of the experimental catchments. Considering  $V_0$  as constant for the whole grid mesh can be partly justified because although velocity is physically dependent on both the slope and the hydraulic radius (among others), the former generally decreases when going downstream whereas the latter increases. Hence, one partly compensates the other.

We carried out additional tests using a geomorphological relationship between velocity and slope, that is,  $V_0 = \mu \times I_a \times S_b$  ( $I$  slope,  $S$  upstream area) for each cell instead of  $V_0 = \text{cte}$ . However, the new formulation did not change the results significantly. Hence, we opted for the simpler formulation and set  $V_0 = 2$  m/s and  $K_0 = 0.7$ .

The kinematic wave is used for the drainage network. The model parameters are mainly  $K_r$  and the dimensions of the cross-section. The velocity is computed using the Manning-Strickler formula (Equation 3). In this application, all cross-sections are considered to be rectangular.

$$V(t) = K_r \times \sqrt{I} \times R_h^{0.66},$$

$$R_h = \frac{H \times W}{2 \times H + W},$$

where  $K_r$  is Strickler roughness coefficient [ $L^{1/3}/T$ ],  $I$  is slope of the channel [ $L/L$ ],  $R_h$  is hydraulic radius [ $L$ ],  $H$  is flow depth [ $L$ ],  $W$  is width of the cross-section [ $L$ ].

In case of the overbank flow, that is, when  $H$  is higher than the canal depth ( $D_c$ ), the cross-section is divided into the stream bed and flood plain (right or left).

### 2.3.1 | Model discretisation and parameterisation

The urban catchment of Bamako has been divided into subcatchments using an urban area threshold of 10 ha, that is, each subcatchment regardless of its size should contain 10 ha of urban landcover. This operation has yielded 1033 units with total areas ranging between 10 and 14,275 ha (Figure 2c). A hydrograph is calculated at the outlet of the subcatchment using the reservoir model coupled to the lag and route transfer function applied to each 10 m cell. It is then injected into the

drainage network and routed using the kinematic wave function (Figure 2b).

The model's parameters have been determined using data from the three experimental catchments. The runoff parameters, that is, ponding loss ( $P_i$ ) and runoff coefficient (RC), have been associated with four types of land use: natural areas, peri-urban areas, urban areas and streams. They have been obtained by minimising the error between the observed and simulated runoff for all the catchments using a trial-and-error procedure. The fact that the experimental catchments had different land use covers guaranteed a robust estimation of the parameters. Although 2 years of monitoring data on three experimental catchments may seem as a small dataset, it is more than the field data that is usually available for urban catchments in Africa. By linking the runoff parameters to land use, the model can be applied not only to the experimental catchments but, more generally, to the entire urban catchment of Bamako.

For the transfer function used to route water in the drainage network, a distinction is made between natural and artificial reaches. For the natural reaches,  $W$  and  $D_c$  are determined using geomorphological formulae based on slope ( $I$ ) and drained area ( $A$ ) and fitted using field survey data. The value chosen for  $K_r$  corresponds to the mean of the value interval usually chosen for natural rivers, that is, between 10 to 30.

$$W = I^{-0.25} \times A^{0.25},$$

$$D_c = 0.5 W^{0.5},$$

$$K_r = 20 \text{m}^{1/3}/\text{s}.$$

The slopes were derived from the DEM analysis. They were smoothed in order to reduce the impact of DEM errors on the slope computation, as the kinematic wave model, is very sensitive to them. For each cell, the slope was computed as the average value of the 50 downstream cells.

$D_c$  and  $K_r$  were determined based on three categories of rectangular ditches. Note that the model is very sensitive to  $K_r$ .

- If  $1 \text{ m} \leq W \leq 5 \text{ m}$ ,  $W = 2.50 \text{ m}$ ,  $D_c = 1 \text{ m}$ ,  $K_r = 30 \text{ m}^{1/3}/\text{s}$ ,
- If  $5 \text{ m} \leq W \leq 10 \text{ m}$  and  $1 \text{ m} \leq D_c \leq 1.5 \text{ m}$ ,  $W = 7.50 \text{ m}$ ,  $D_c = 1.25 \text{ m}$ ,  $K_r = 50 \text{ m}^{1/3}/\text{s}$ ,
- If  $10 \text{ m} \leq W \leq 20 \text{ m}$  and  $1 \text{ m} \leq D_c \leq 2 \text{ m}$ ,  $W = 15 \text{ m}$ ,  $D_c = 1.50 \text{ m}$ ,  $K_r = 50 \text{ m}^{1/3}/\text{s}$ .

## 2.4 | The experience feedback's cartographic method

On 17 May 2019, in the immediate aftermath of the flood event, 10 teams of students from the Laboratoire Hommes-Peuplements–environnements (lobo-hope) of USSGB were sent into the field to collect data about the flooding processes and mechanisms as well as the economic losses and damages.

The city was divided into 10 districts for data collection. Students were asked to map the flooded area in collaboration with the local communities but also to document flood depth and overbank water depth by reporting water high marks on the walls and trees. The districts were delineated using the Fieldpapers application (OSM), and the flooded areas were mapped directly into Fieldpapers using GPS. The spatial extent of the floods was delineated with the help of the local communities who also confirmed the flood depths. Back at the laboratory, the printed and documented Fieldpapers maps were scanned and uploaded onto the Fieldpapers website (<https://fieldpapers.org/>) to automatically produce the maps of the flooded areas.

## 3 | RESULTS AND DISCUSSION

### 3.1 | Modelling results on three experimental catchments

Over the monitoring period, 10, 8 and 9 events were recorded with an average rainfall  $>20$  mm over the catchments of Faladié, Cité Niger and Bolibana, respectively (Table 3). The maximum rainfall is 65, 44 and 57 mm, respectively. The averaged runoff coefficients are 0.56 and 0.38 in Cité Niger and Faladié, respectively, but only 0.08 in Bolibana as a consequence of a lower urbanisation. The maximum peakflow values are recorded for the event of 13 July 2017 when peakflow reached  $31.7 \text{ m}^3/\text{s}$  in Faladié,  $23.2 \text{ m}^3/\text{s}$  in Bolibana and  $20.2 \text{ m}^3/\text{s}$  in Cité Niger. These values correspond to specific discharge values of 4.3, 0.5 and  $5.9 \text{ m}^3/\text{s}/\text{km}^2$ .

A good linear regression ( $0.66 \leq R^2 \leq 0.84$ ) is obtained between the measured and calculated runoff per event on these catchments (Figure 3) when using the parameters fitted to the experimental data by trial and error:

$P_i = 5 \text{ mm}$  and  $RC = 0.6$  for urban cells or stream cells,

$P_i = 10 \text{ mm}$  and  $RC = 0.2$  for periurban cells,

$P_i = 20 \text{ mm}$  and  $RC = 0.05$  for natural cells.

These values are used for individual cells throughout the study zone. With hindsight it appears that the RC values obtained by spatially distributing the production function are close to the 1st quartile of the calculated RC

values presented in Table 3 for the Faladié (peri-urban) and Bolibana (natural) catchments: respectively, 0.18 versus 0.2 and 0.04 versus 0.05, respectively. The fitted values are however closer to the third quartile of the RC values of Cité Niger (Table 3): 0.55 versus 0.6. Since some of the events measured on the experimental catchments were used in the trial-and-error procedure, some connection between the fitted and calculated RC values is to be expected.

The linear regressions between the measured and calculated runoff (Figure 3a) have slope values close to 1 and intercept values close to 0 for Faladié and Bolibana. However, the runoff was substantially underestimated by the model. A hypothesis for this underestimation is that the catchment boundaries were not correctly defined. This often occurs in urban hydrology, either in flat areas or when the channels or drainage works are not efficient because of clogging or litter accumulation. Another common cause for the underestimation of runoff is the use of low or average intensity rainfall events, having lower runoff coefficients, during the calibration phase. Nevertheless, we do not think that this argument is valid in our case. Indeed, heavy rainfalls ( $\sim 80$ – $100 \text{ mm}$ ) were measured on the experimental catchments, and the corresponding events were used during the model set up. These events did not have higher runoff coefficients than medium rainfall events. Similarly, the linear regressions between the measured and calculated peak flows (Figure 3b) show an underestimation of the peak flows calculated by the model in Cité Niger, while those of Faladié and Bolibana are correctly simulated. Note that the measured and calculated peak flows in Bolibana have the lowest  $R^2$  value of  $\sim 0.39$ , which is most probably due to (i) the more complex behaviour of peri-urban areas where natural zones alternate with impervious surfaces and (ii) the spatial variation of rainfall and the uncertainties related to rainfall estimations over this large catchment. Additional data may be necessary to better understand and quantify the response of the natural zones located in peri-urban areas.

We have carried out various tests (although the results are not presented herein) to improve these results. We tested alternative production and transfer functions (Soil Conservation Service; SCS, Clark's unit hydrograph, a geomorphological formulation of the Lag and Route function), a lumped versus a distributed approach, and of course also tested other parameter values. Despite our best efforts, the results could not be improved. We thus think that these results might be explained by delimitation problems due to the quality and the resolution of the DEM we had access to, measurement errors in discharge data, and a poor spatial estimation of the precipitation. Indeed, had the problem been related to the structure of the model or the choice of the parameters, our tests

TABLE 3 Main characteristics of the rainfall-runoff events

Date	P (mm)	R (mm)	Q <sub>mes</sub> (m <sup>3</sup> /s)	RC (%)
(a) Bolibana				
13 Jul 2017	32.6	3.5	23.2	0.11
20 Jul 2017	34.2	2.1	11.3	0.06
24 Jul 2017	24	0.5	4.1	0.02
26 Jul 2017	0.6	0.5	1.6	0.83
29 Jul 2017	45.7	0.9	7.1	0.02
31 Jul 2017	41.4	4	10.9	0.1
06 Aug 2017	32.7	1.9	7.3	0.06
08 Aug 2017	17.5	0.7	8.3	0.04
09 Aug 2017	11.9	1.5	1.8	0.13
11 Aug 2017	4.6	0.6	1.8	0.13
14 Aug 2017	19.7	1.3	11.1	0.07
15 Aug 2017	38.2	3.4	22.5	0.09
18 Aug 2017	12.9	1.5	12.7	0.12
22 Aug 2017	36.8	3.3	10.3	0.09
27 Aug 2017	19.6	1.9	6.9	0.1
30 Aug 2017	14.6	0.2	3.7	0.01
31 Aug 2017	19.8	1.3	8.4	0.07
01 Sep 2017	57	5.9	15.5	0.1
09 Sep 2017	7.8	0	5.5	0
11 Sep 2017	7	0.4	7.9	0.06
16 Sep 2017	9.4	0	4.2	0
(b) Faladié				
13 Jul 2017	35.2	19.1	31.7	0.54
20 Jul 2017	25.9	7.3	8.4	0.28
24 Jul 2017	14.9	2.1	2.5	0.14
26 Jul 2017	9.5	3.1	4.2	0.33
29 Jul 2017	24.9	5.8	7	0.23
31 Jul 2017	28.6	9.3	10.1	0.33
06 Aug 2017	65	22.7	26.2	0.35
08 Aug 2017	5	2.2	1.5	0.44
09 Aug 2017	24.3	11.5	17	0.47
11 Aug 2017	6.5	0.9	1	0.14
14 Aug 2017	13.9	4.5	8.9	0.32
15 Aug 2017	27.6	12.6	15.4	0.46
18 Aug 2017	10.3	1.6	2.8	0.16
22 Aug 2017	19.1	5	6.1	0.26
27 Aug 2017	29.5	9.5	8.7	0.32
30 Aug 2017	10.8	1.4	2.6	0.13
31 Aug 2017	2.4	0.3	0.2	0.13
01 Sep 2017	40.1	14.4	28.9	0.36
09 Sep 2017	11.8	3.4	7	0.29
11 Sep 2017	8.7	2.9	5.5	0.33
16 Sep 2017	42	7.4	11.1	0.18



TABLE 3 (Continued)

Date	P (mm)	R (mm)	Q <sub>mes</sub> (m <sup>3</sup> /s)	RC (%)
(c) Cité Niger				
13 Jul 2017	37.6	33.5	20.2	0.89
20 Jul 2017	11.4	4.9	4.3	0.43
24 Jul 2017	12.1	3.6	1.8	0.3
26 Jul 2017	1.4	0.7	0.5	0.5
29 Jul 2017	15.4	3.1	2	0.2
31 Jul 2017	32.6	13.3	10.9	0.41
06 Aug 2017	28.1	11.8	3.3	0.42
08 Aug 2017	15.3	5.1	3.5	0.33
09 Aug 2017	13.4	10.8	3.1	0.81
11 Aug 2017	4.7	0.6	0.2	0.13
14 Aug 2017	18.1	11.1	8.6	0.61
15 Aug 2017	36.6	18.6	10.2	0.51
18 Aug 2017	41.2	14.1	7.8	0.34
22 Aug 2017	34.4	19.5	7.3	0.57
27 Aug 2017	44	24.4	9.2	0.55
30 Aug 2017	3	1.1	0.5	0.37
31 Aug 2017	9.8	4	1.5	0.41
01 Sep 2017	31.8	20.7	4.1	0.65
09 Sep 2017	5.1	8.6	1.8	1.69
11 Sep 2017	7	2.2	2	0.31
16 Sep 2017	5.8	0.5	0.4	0.09

would have yielded better results, yet this was not the case.

### 3.2 | Validation: Experience feedback on the 16 May 2019 flood event

#### 3.2.1 | Synoptic situation

The event of 16 May 2019 was produced by a Mesoscale Convective System (MCS). These systems are the main contributors of annual rainfall during the rainy season (April–September) in the Sahel region (Le Barbé et al., 2002; Mathon et al., 2002). MCSs are composed of a front of convective cells associated with high rain rates followed by a rear stratiform with low to medium rainfall rates. Recent studies have pointed out the increase in extreme events in the Sahel probably due to climate change (Panthou et al., 2018; Taylor et al., 2017). Such an increase added to a change in land use can lead to more frequent flooding.

The MCS that caused the extreme precipitation event over Bamako on 16 May 2019 was relatively small and

had a short lifetime cycle of a few hours. The system originated from the remnants of an easterly disaggregated MCS. Figure 4 shows the Multi-Sensor Precipitation Estimate (MPE) product from EUMETSAT at different time steps. At 02:00 h UTC, we observe the dispersed patches of low rainfall (in grey) from a previous MCS over the Segou region, northeast of Bamako. At 03:00 h UTC, the MCS causing the flood in Bamako starts growing near Koulikoro, about 50 km northeast of Bamako. At 04:45 h, the system is situated over Bamako with a clear band on intense convective rainfall rates. At 08:20 h UTC, the system shows no more convective rainfall rates and disaggregates near the border of Guinea. The MPE precipitation product is based on Meteosat infrared observations (IR) from a geostationary orbit (36,000 km) corrected with microwave low orbit satellites. As it relies on IR, it is associated with high uncertainty compared to microwave products (Gosset et al., 2018; Satgé et al., 2020). Nevertheless, it has the benefit of the IR resolution and the 15 min time frequency. In this study, the MPE is used qualitatively only to show the MCS structure and evolution at the mesoscale. For the EWS, we used the available rain gauges,

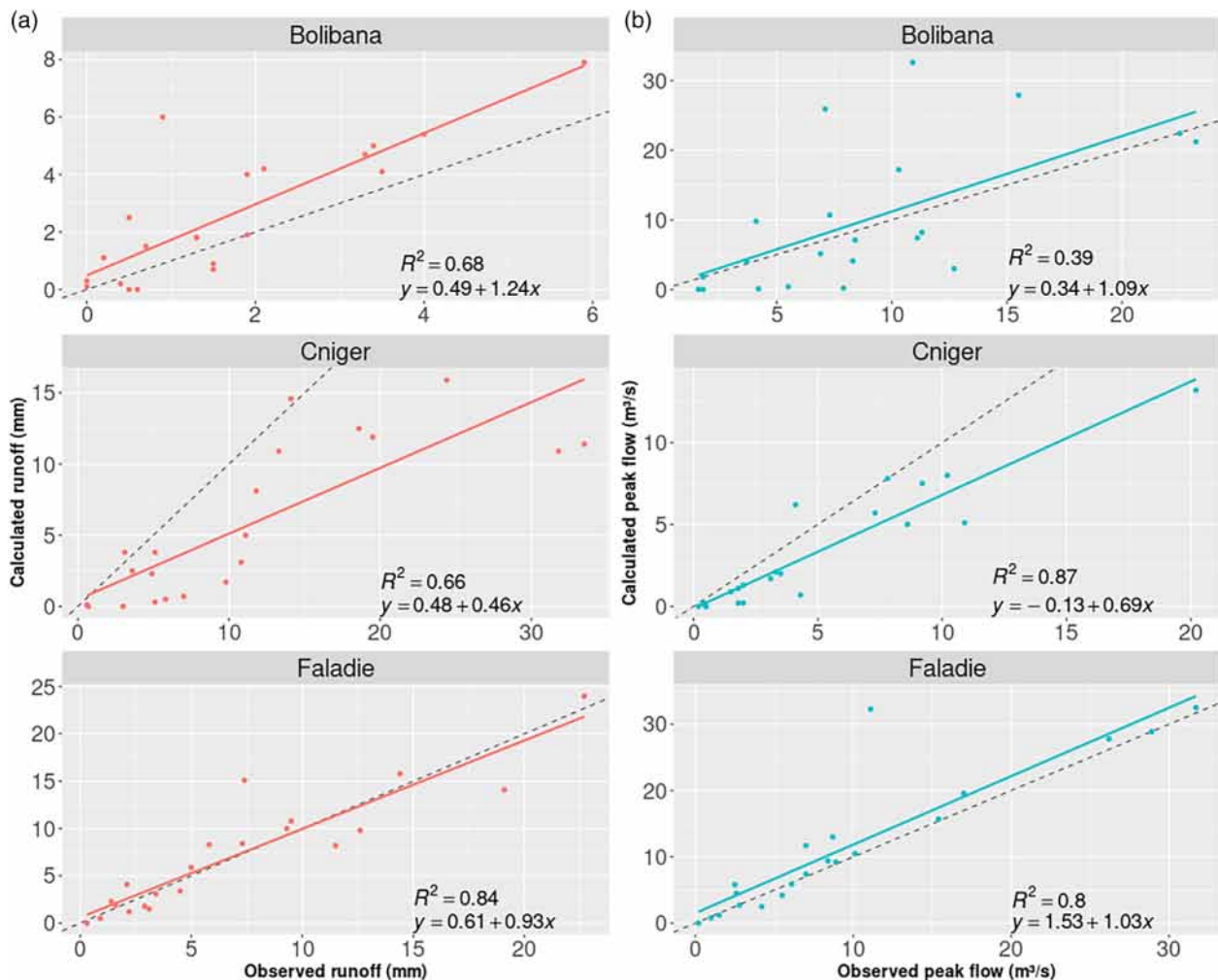


FIGURE 3 Scatterplots of calculated and measured runoff (a) and maximum peak flow (b) for the three studied catchments. The dashed lines represent the identity (1–1) lines, the continuous lines are the fitted regression lines.

which when combined, provide unbiased, real time rainfall measurements.

The reference rainfall satellite products are based on microwave observations but have a coarser resolution and depend on the flyby of the satellites during the event to capture microwave rainfall signatures. The Integrated Multi-satellitE Retrievals for GPM (IMERG) product (Huffman et al., 2019) that merges all the microwave satellites and IR observations estimated 40 mm of rainfall for the considered event in Bamako. The ERA5 model reanalysis (Hersbach et al., 2020) did not show any rainfall for the event due to the difficulty models have in predicting rainfall in general and the short lifetime of the present MCS in particular.

### 3.2.2 | Rainfall data

Five rain gauges were used to feed the EWS in real time. The gauges were equipped with 0.5 mm tipping buckets

and a teletransmission system via the GSM network. They were calibrated biweekly, and a totalizer container buried next to it served as a reference for tipping drift correction. Their locations are shown in Figure 1. Data from three additional daily rain gauges from MALI-METEO are also used in this analysis, but only five among the eight gauges were used in real time at a 5-min step.

The gauges started recording the 16 May event at 03:26 h and stopped at 06:35 h local time (UTC). Figure 5 presents the rainfall accumulation for the case study event at each gauge location and its interpolation using Thiessen polygons: the gauges situated in the North East of Bamako showed accumulations greater than 100 mm, with a maximum of 138 mm for a single gauge. The highest recorded rain rate at a 5-min time step is 132 mm/h at 04:55 h local time.

MALI-METEO has a long series of observations in the country starting in the early 1950s. To put into perspective the rainfall amount observed in Bamako for the studied event, the total rainfall was compared to both the

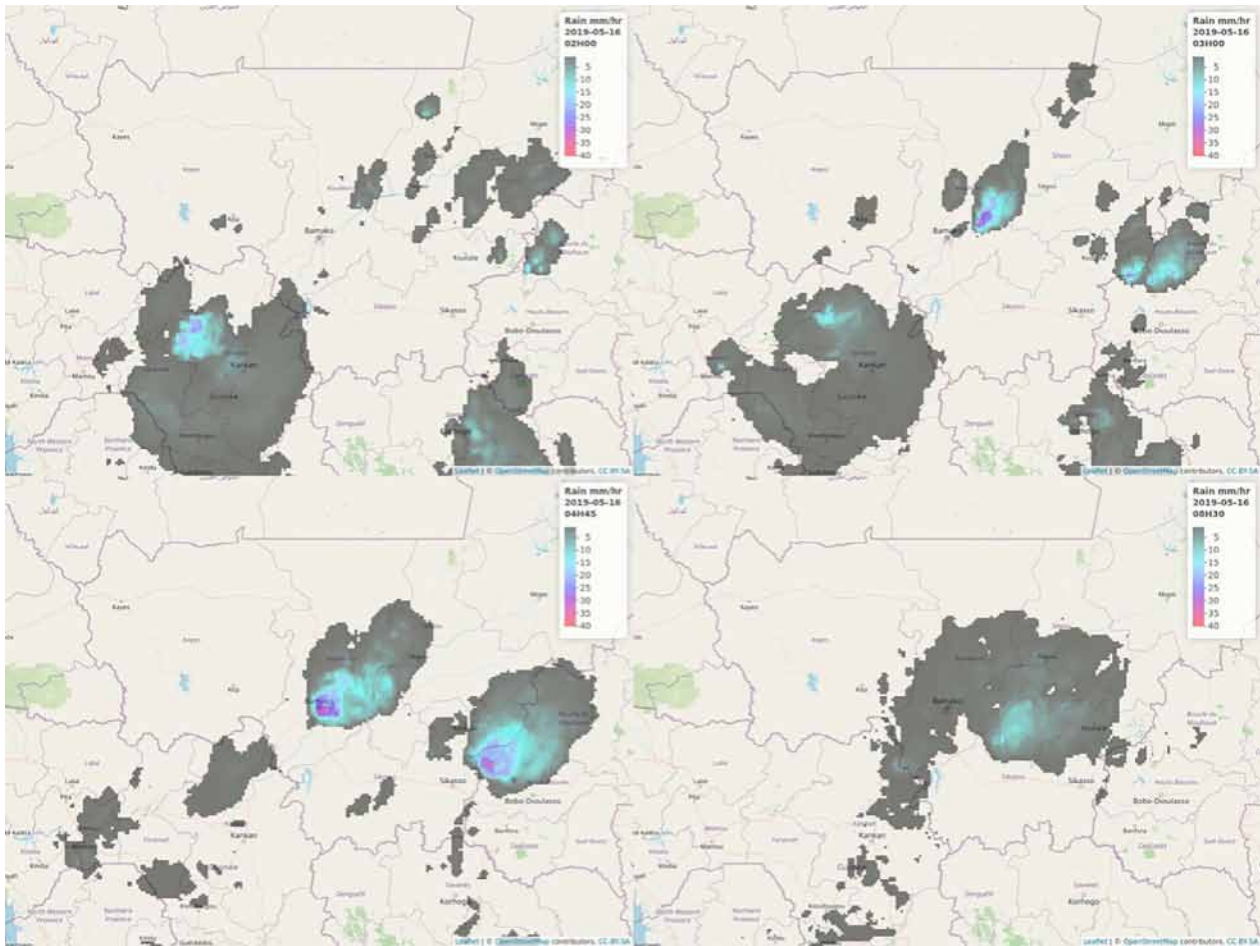


FIGURE 4 The precipitation values estimated by the MPE (EUMETSAT) product for the 16 May 2019 event.

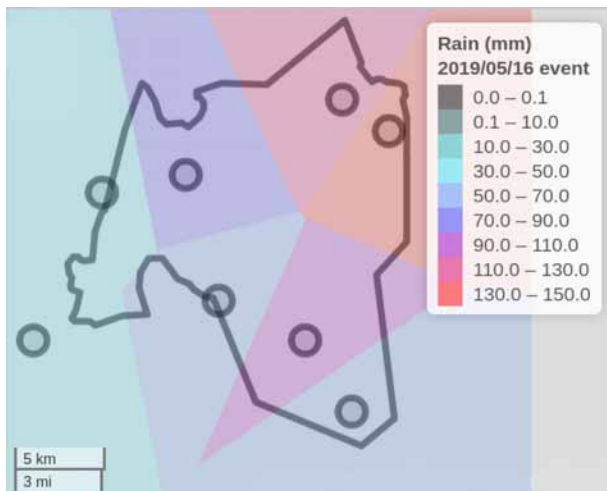


FIGURE 5 Measured and interpolated rainfall for the 16 May 2019 event.

historical series of 2-day accumulation maximums and to the monthly maximum rainfall. We chose 2 days as an MCS event can last a maximum of 2 days. The number of

gauges in the Bamako time-series varies over the years from 2 to 4. For over more than 60 years, only five historic events overcame the studied one.

The present case study highlights the need for rainfall measurements at high spatial resolutions for urban hydrology applications. Satellite data (IMERG) at a 10 km resolution is not fine enough to detect the urban variability of rainfall for such events, which leads to highly variable water outflow in the city. Current projects such as HYDROMET Africa funded by the World Bank aim to endow meteorological radars to West African meteorological agencies to fill the rainfall data gap.

### 3.2.3 | Flood modelling

Data from five rain gauges were used to run the hydrological model using the parameters previously determined at the scale of the experimental catchments (Figure 1). No further calibration was carried out using water level or discharge data. Figure 6 presents the rainfall input of the hydrological model and the simulated

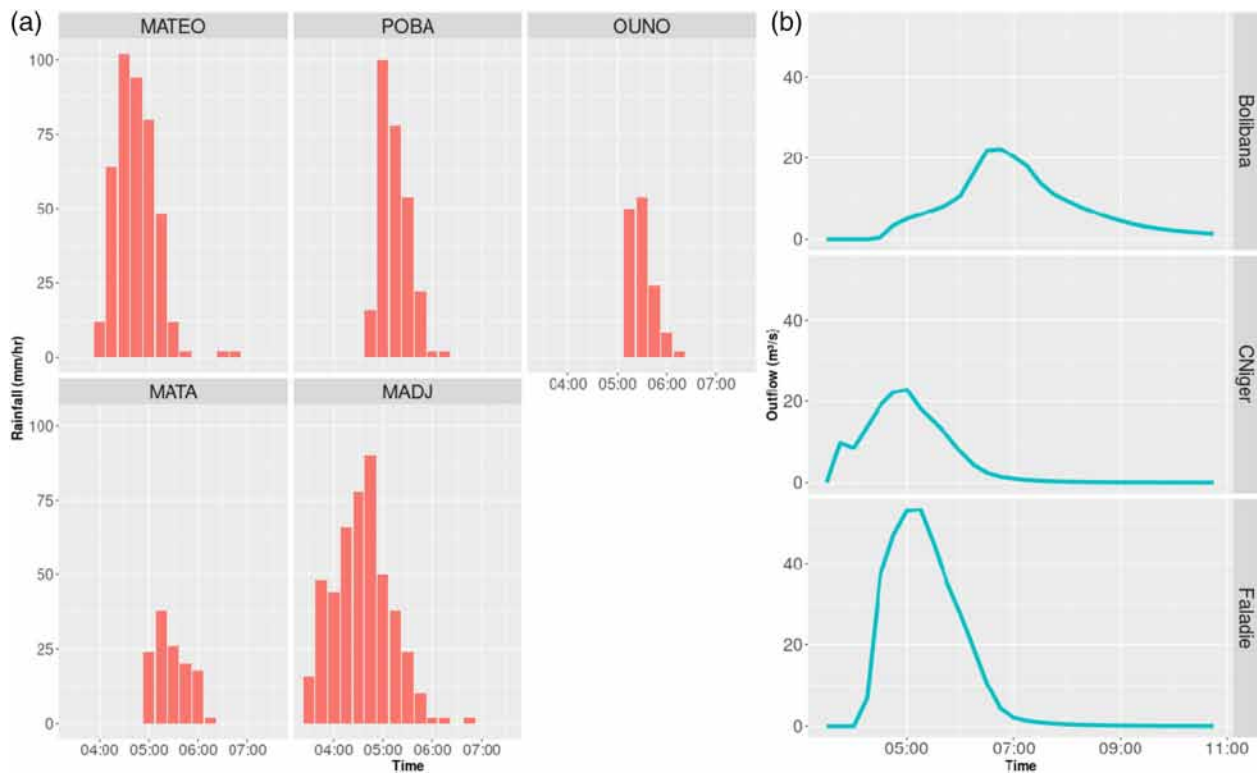


FIGURE 6 Rainfall hyetograms used as modelling inputs and simulated hydrographs at the outlets of the three experimental catchments.

discharge at the outlet of the experimental catchments. It can be seen that Faladié has the flashiest response and highest peakflow value ( $53.2 \text{ m}^3/\text{s}$ ), while Bolibani has the slowest response and lowest peakflow value ( $22.2 \text{ m}^3/\text{s}$ ). This is due to the type and size of the catchment's land use but also to the spatial distribution of the rainfall, as the rain gauges located closest to the Bolibani have recorded the lowest rainfall intensities (Figure 6). The lag times calculated using the closest rain gauges are of 30 min for Faladiyé, 15 min for Cité Niger and 105 min for Bolibana.

The peakflow values simulated for the event reached  $81.9 \text{ m}^3/\text{s}$  in the districts located on the left bank of the Niger River and  $143 \text{ m}^3/\text{s}$  in those located on the right bank (Figure 7). The former had more locations where the overbank flow was simulated (Figure 8), namely, in the vicinity of the Sotuba, Molobalini and Djelibougua collectors in District I and Quinzambougo in District II. The highest peakflow values were simulated at Molobalini. In comparison, despite higher peakflow values, overbank flow was simulated only at two locations on the right bank, namely, at the junctions of the Unité Africaine Avenue, the Faladié collector and the Niakamoro borough and further to the west in District VI in the Kalaban Koura borough along the banks of the Soganiko River.

These hotspots correspond to the flooded areas reported by the rapid Post-Disaster Needs Assessment (PDNA), which has also reported flooding in the vicinity of the Yirimadio—Missabougou natural collector in District VI (Republic of Mali, 2019). According to the same source, water levels reached 1.5–2 m in some streets of Missabougou (Republic of Mali, 2019). The Missabougou collector is located underneath an irrigation canal, and its section is often modified because of litter deposit. This may explain why despite high discharge values, the model did not simulate overbank flow at this location. It should be noted that  $K_r$  values were based on the original material of the channel bed and bank material as the degree to which a channel is congested is assimilated to its initial condition. It is variable in time and currently there is no video surveillance of the channels to provide this information. It is also possible that the simulated peakflow values were lower than the real ones because of the model's tendency to underestimate peakflow, as highlighted on the three experimental catchments.

### 3.2.4 | Field survey map

The map elaborated by the USSGB shows the extent of the flooded areas along the natural rivercourses

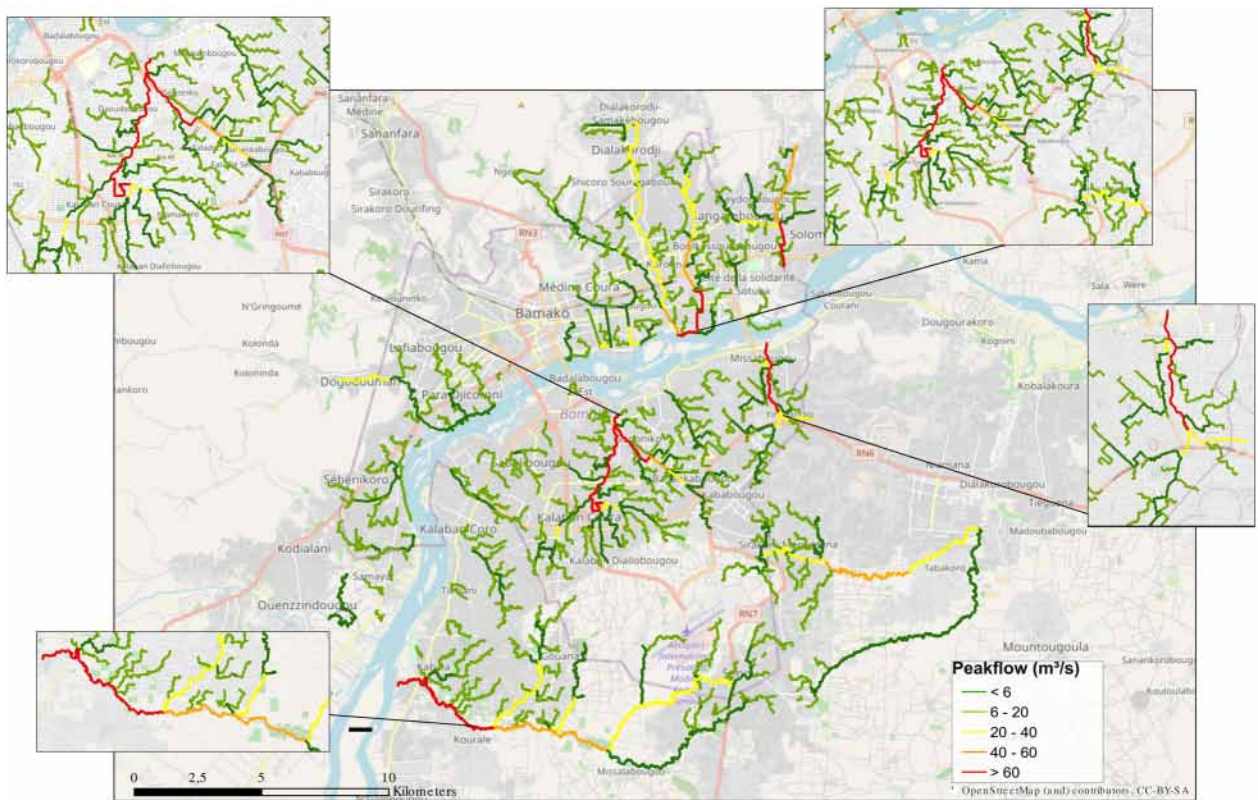


FIGURE 7 Map of peakflow values calculated for the event ( $m^3/s$ ).

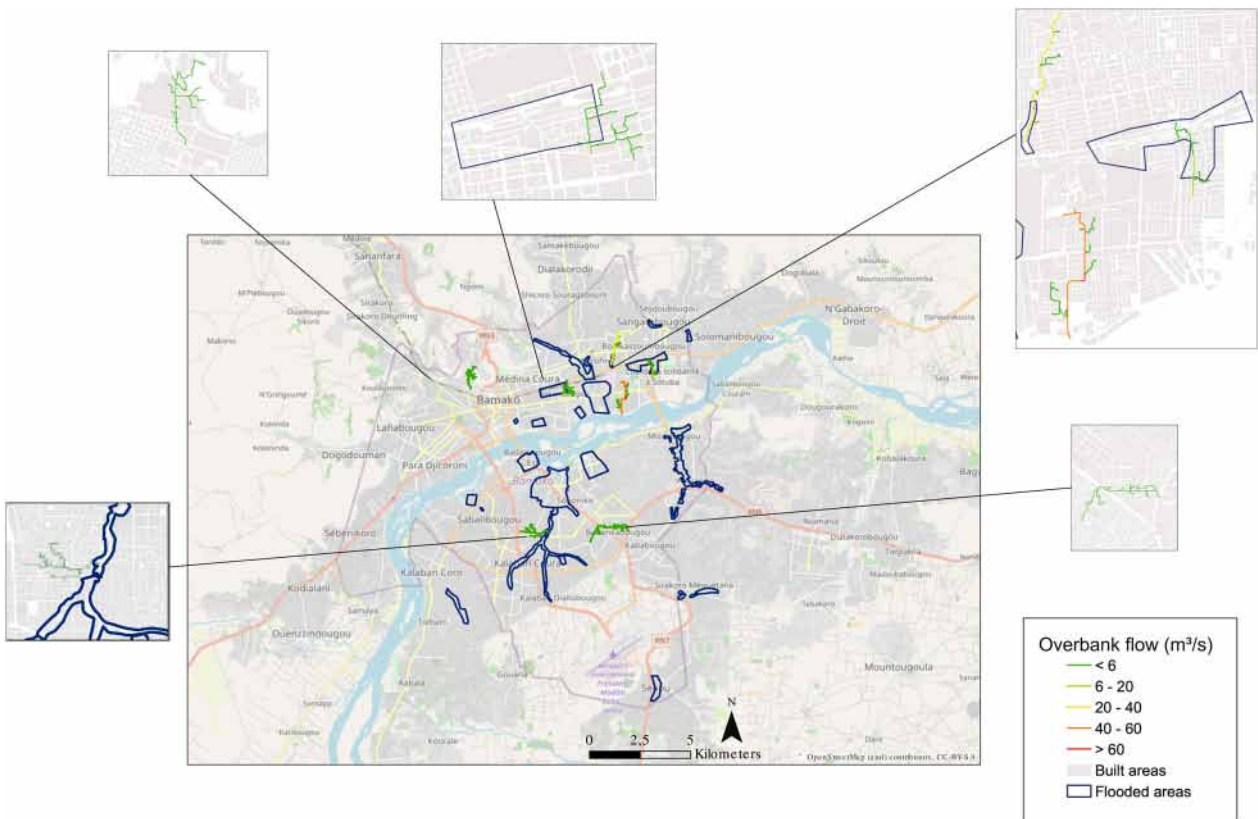


FIGURE 8 Comparison between the simulated overbank flow and the map of the flooded areas reported in the USSGB rex experiment. Overbank flow is calculated as the difference between calculated peakflow and maximum peakflow capacity of the drainage network ( $m^3/s$ ).

(Figure 8). This is a clear addition to the model's output, as in its current version, the simulation model only allows one-dimensional (1D) transfer, and hence, the lateral extension of the flood cannot be mapped. The flooded areas are mainly located in the eastern part of the catchment. The model has correctly identified most of the spots located on the left bank of the river but missed some of those located on the right bank. High peakflow values were, nevertheless, simulated for some of these locations, namely, along the watercourse near Kouralé and Sabakouro (Figures 7 and 8). We hypothesise that the flooding may have been caused by solid waste disposal in the dried up river beds and collectors, a widespread phenomenon in Bamako, which would have narrowed the flow section (Figure 9a). This highlights the need for constant surveys on the flow conditions throughout the drainage network.

Based on the field surveys, the total flooded areas amount to 14.6 km<sup>2</sup>. This is in accordance with the number of partially or totally damaged houses, that is, 124 units, reported in the Rapid PDNA report. More than 95% of the crumbled houses are traditional houses made of mud and thatch (banco) and correspond to informal



**FIGURE 9** (a) Example of a collector clogged by litter at Cité Niger, Bamako (12.642591, -7.976238). Photo taken on 20 May 2017. Copyright F. Cazenave. (b) Example of a house built in the inundation bed in Bamako (12.681323, -7.922695). Photo taken on 28 April 2016. Copyright F. Cazenave.

settlements located either in the river's inundation bed or in its vicinity (Republic of Mali, 2019). Field observations have shown that houses made of concrete walls are also built in the riverbed and act locally like a dam, making water levels rise and neighbouring mud houses collapse (Figure 9b). Thus, the damage caused by the floods is due to both the conjunction of an extreme rainfall event of short duration and the obstruction and clogging of the waterways. Hence, monitoring only rainfall and water levels in streams is not a sufficient means to avoid further floods. As already advocated for by previous reports, specific measures should be taken, including educational programmes to reduce waste deposits in the collectors and natural rivers and avoiding all types of constructions in flood prone areas, namely, in the rivers' inundation beds and flood plains surrounding them. This has been identified as an anthropic factor contributing to flood increases in the Sahel (Descroix et al., 2017).

Additional knowledge on the flood generation mechanisms is also necessary. In comparison with traditional African housing or European style constructions for which runoff mechanisms have been documented with experimental data and modelling results (Bouvier et al., 2018; Hingray et al., 2000), there is a clear lack of knowledge regarding runoff genesis, propagation, and modelling in informal settlements. This is an example of new research that could help flood risk management in Africa and that needs to be led by African institutions (Lumbroso, 2020; Odume & Slaughter, 2018).

## 4 | CONCLUSIONS AND PERSPECTIVES

The devastating flood event of 16 May 2019 is a good case study of the adaptability required from an EWS. Indeed, given the synoptic situation and the storm's development pattern, none of the global forecasting systems were able to foresee its occurrence and magnitude. In this configuration, alternative, more local rainfall measurement techniques such as those based on commercial microwave links' (CML) signal attenuation could be the answer. This technique was tested successfully to estimate the rainfall in West Africa (Gosset et al., 2015). In addition, simulations showed its relevance in hydrological applications at the city scale (Turko et al., 2021; Pastorek et al., 2019; Fencil et al., 2013; Fencia et al., 2012). The technique allows real-time country-wide nowcasting, as experienced in Germany and the Netherlands (Chwala et al., 2019; Imhoff et al., 2020). In dense zones like Bamako CMLs may improve rainfall sampling and flood simulation.

Although the EWS did not run in real-time during the event, the hydrological model developed as part of

the Raincell App demonstrator correctly identified most of the locations where overbank flow occurred in hindsight. In the absence of discharge and water level data, the predicted discharge and volume values cannot be validated. However, in view of the water levels reported both in the PDNA report (Republic of Mali, 2019) and during the field survey carried out by the USSGB, they are realistic and plausible. The modelling approach we used has, of course, its limitations; the main one is that at the time being, it identifies overbank flow locations along the drainage network but does not propagate the flow laterally. Hence, in its current version, it cannot be used to delimit flooded areas unless it is coupled to a 2D hydraulic model. As part of a new research project, our model is being coupled to HEC-RAS. This is not a straightforward task: in addition to combining discretisation schemes and ensuring numerical stability, it requires the use of high-resolution elevation data. This is one of the main challenges that needs to be addressed in African cities where in the absence of other alternatives, modelling is often carried out using open access global DEMs. Indeed, although Azizian and Brocca (2020) showed that ALOS-PALSAR gave similar results to a ground DEM for 1D hydraulic modelling of floods in data scarce regions, our experience on Bamako showed it produces noisy slope maps.

A good representation of the spatial variability of rainfall is also mandatory for an accurate simulation of discharge. The distributed rainfall-runoff model scheme used for the EWS is sensitive to the spatial variability of rainfall, as highlighted by Trambly et al. (2011) using radar rainfall fields and, more recently, by Turko et al. (2021) using CMLs of variable density. The latter is particularly interesting, as it was carried out in a similar urban setting in West Africa (Ouagadougou). Turko et al. (2021) showed that peak discharge may be overestimated by a factor close to 2 and, in some instances, underestimated by a factor of 3 based on network. These results may have been enhanced by the nonlinearity of the model equations that had been used (SCS); they nevertheless highlight the discretisation scheme's sensitivity to rainfall. The hydrological model used in this EWS, as all models, is a simplification of reality built on given hypotheses, such as a runoff coefficient that is constant in time. The model was kept simple in order to avoid over-parameterisation and equifinality problems. Our current dataset supports the hypothesis made on the runoff coefficient. However, it only covers 2 years of monitoring at three locations. It would be advisable to couple discharge and water level monitoring to the already existing rainfall surveillance scheme and increase the dataset that may be used for model fitting.

It is worth noting that some of the locations identified by the EWS, namely, Djelibougua and Sotuba in District

I and Missabougou in District VI, had already been identified as flood prone areas that have vulnerable equipment by a report handed to the authorities in May 2019 (SOMAGEF, 2019). Interestingly enough, another flood prediction demonstrator was funded by international donors and produced a report approximately at the same period (Seidou & Diabété, 2019). Despite these two demonstrators and at least three technical reports, human lives were still lost during the flood event. During the USSGB fieldwork, residents reported that the flood event occurred so rapidly that the DGPC did not have time to reach the flooded areas where water levels reached 3 m in some locations. The ground floors of all the houses were flooded, and despite admirable solidarity between residents, human lives were lost. The EWSs developed for Bamako have focused on the Niger River and on fluvial flood risk. In Bamako and in many other Malian towns such as Djénné, Bla, Sofra and Sikosso, the tributaries and canals that cross the cities are not monitored even though they are known to induce urban floods caused either by the upwelling of the Niger River when it is in high flows or through runoff as it occurred during the 19 May 2019 event. Indeed, the Niger was in low flow conditions during the event, and the flood was caused by a very high intensity and short duration rainfall event that none of the weather forecasting systems had detected. In such conditions, flood prediction platforms that do not rely on real-time rainfall monitoring, such as the one reported in Seidou and Diabété (2019), would be of little use. Short-term forecasts (1–3 h) would allow a significant increase in 'lead time', thus giving the population more time to protect their property and increasing their trust in the system (Rai et al., 2020). However, on catchments that have an extremely rapid response and for flash floods, the use of forecasts based on satellite or radar images would affect the accuracy of the flood forecast (AIDR, 2009). Despite a lead time of less than an hour, the authorities have the possibility of alerting the population by SMS broadcast or by activating the sirens implemented in the areas at risk.

The flanking measures recommended by the rapid PDNA report include the need to implement modern flood management tools, such as EWSs, databases, emergency operations' centres, and digital maps (Republic of Mali, 2019). It should, however, be noted that these measures will have even greater impact if information is automatically shared between all the stakeholders involved in flood risk management, on the one hand, and the local populations, on the other. Timely sharing of warnings with the latter is of course of paramount importance. However, the decision to alert the populations falls within the responsibility of the designated authorities and does not rely solely on a fully automated system. The experts who are part of the crisis management use the

EWS as an indicator but rely also on their own knowledge to advise the authorities. The population's response will be conditioned by the clarity of the information, the way it is disseminated, their trust in the source but also by their perception of the threat (Golding, 2009; Perera et al., 2020). Within the PGCRI project framework (Projet de Gestion des Risques climatiques et d'Inondations au Mali), guidelines for an educational programme to raise awareness of climate change and flood risks have been established (Republic of Mali, 2020). Hopefully, their benefits will be visible in the forthcoming years.

## ACKNOWLEDGEMENTS

This work was funded by the Korean Green Growth Fund (KGGTF, a trust fund managed by the World Bank, selection 1212152). The authors wish to thank Anne Crespy for the Linux version of the rainfall-runoff model.

## DATA AVAILABILITY STATEMENT

The data that support the findings of this study are openly available in « Raincell\_mali » at <https://dataverse.ird.fr/>, reference numbers 10.23708/RXSSDX, 10.23708/ZI0ONV, 10.23708/DNVAAI, 10.23708/PDLP9F, 10.23708/CL3VFS.

## ORCID

Nanée Chahinian  <https://orcid.org/0000-0002-0037-5377>

## REFERENCES

- AIDR-Australian Institute for Disaster Resilience. (2009). Australian disaster resilience handbook collection flood warning. Manual 21. <http://www.dpmc.gov.au/>
- Alfieri, L., Zsoter, E., Harrigan, S., Aga Hirpa, F., Lavaysse, C., Prudhomme, C., & Salamon, P. (2019). Range-dependent thresholds for global flood early warning. *Journal of Hydrology X*, 4, 100034. <https://doi.org/10.1016/j.hydroa.2019.100034>
- Azizian, A., & Brocca, L. (2020). Determining the best remotely sensed DEM for flood inundation mapping in data sparse regions. *International Journal of Remote Sensing*, 41(5), 1884–1906. <https://doi.org/10.1080/01431161.2019.1677968>
- Bouvier, C., Chahinian, N., Adamovic, M., Cassé, C., Crespy, A., Crès, A., & Alcoba, M. (2018). Large-scale GIS-based urban flood modelling: A case study on the City of Ouagadougou in Gourbesville. In P. Gourbesville, J. Cunge, & G. Caignaert (Eds.), *Advances in Hydroinformatics* (pp. 703–717). Springer.
- Bouvier, C., & Delclaux, F. (1996). ATHYS: A hydrological environment for spatial modelling and coupling with a GIS. In K. Kovar & H. P. Nachtnebel (Eds.), *Application of geographic information systems in hydrology and water resource management* (pp. 19–28). IAHS.
- Chitwatkul Siri, D., Miyamoto, H., & Weesakul, S. (2021). Development of a simulation model for real-time urban floods warning: A case study at sukhumvit area, Bangkok, Thailand. *Water*, 13(11), 1458. <https://doi.org/10.3390/w13111458>
- Chwala, C., Smiatek, G., & Kunstmann, H. (2019). Real-time country-wide rainfall derived from a large network of commercial microwave links in Germany. *Geophysical Research Abstracts*, 20, 10096.
- Descroix, L. (2018). Processus et enjeux d'eau en Afrique de l'Ouest soudano-sahélienne. Editions des archives contemporaines/IRD Editions. <https://www.archivescontemporaines.com/books/9782813003140>
- Descroix, L., Mahé, G., Olivry, J., Albergel, J., Tanimoun, B., Amadou, I., & Diedhiou, A. (2017). Chapter 7. Anthropogenic and environmental factors involved in the increase in flooding in the Sahel. In *Rural societies in the face of climatic and environmental changes in West Africa* (pp. 145–161). OpenEdition Books. <https://doi.org/10.4000/books.irdeditions.12343>
- Di Baldassarre, G., Montanari, A., Lins, H., Koutsoyiannis, D., Brandimarte, L., & Blöschl, G. (2010). Flood fatalities in Africa: From diagnosis to mitigation. *Geophysical Research Letters*, 37, L22402. <https://doi.org/10.1029/2010GL045467>
- Egbinola, C. N., Olaniran, H. D., & Amanambu, A. C. (2017). Flood management in cities of developing countries: The example of Ibadan, Nigeria. *Journal of Flood Risk Management*, 10(4), 546–554. <https://doi.org/10.1111/jfr3.12157>
- Emerton, R. E., Stephens, E. M., Pappenberger, F., Pagano, T. C., Weerts, A. H., Wood, A. W., Salamon, P., Brown, J. D., Hjerdt, N., Donnelly, C., Baugh, C. A., & Cloke, H. L. (2016). Continental and global scale flood forecasting systems. *Wiley Interdisciplinary Reviews: Water*, 3(3), 391–418. <https://doi.org/10.1002/wat2.1137>
- Fencl, M., Rieckermann, J., Schleiss, M., Stránský, D., & Bareš, V. (2013). Assessing the potential of using telecommunication microwave links in urban drainage modelling. *Water Science and Technology*, 68(8), 1810–1818. <https://doi.org/10.2166/wst.2013.429>
- Foehn, A., García Hernández, J., Schaeffli, B., & de Cesare, G. (2018). Spatial interpolation of precipitation from multiple rain gauge networks and weather radar data for operational applications in alpine catchments. *Journal of Hydrology*, 563, 1092–1110. <https://doi.org/10.1016/j.jhydrol.2018.05.027>
- Garcia, F. C. C., Retamar, A. E., & Javier, J. C. (2016). A real time urban flood monitoring system for metro Manila. IEEE Region 10 Annual International Conference, Proceedings/TENCON, 2016. <https://doi.org/10.1109/TENCON.2015.7372990>
- Golding, B. W. (2009). Review long lead time flood warnings: Reality or fantasy? *Meteorological Applications*, 16, 3–12. <https://doi.org/10.1002/met.123>
- Gosset, M., Alcoba, M., Roca, R., Cloché, S., & Urbani, G. (2018). Evaluation of TAPEER daily estimates and other GPM-era products against dense gauge networks in West Africa, analysing ground reference uncertainty. *Quarterly Journal of the Royal Meteorological Society*, 144, 255–269. <https://doi.org/10.1002/qj.3335>
- Gosset, M., Cazenave, F., Zougmore, F., Doumounia, A., & Kakou, M. (2015). Rainfall measurements from cellular networks microwave links: An alternative ground reference for satellite validation and hydrology. *Geophysical Research Abstracts*, 17, 4867.
- Hally, A., Caumont, O., Garrote, L., Richard, E., Weerts, A., Delogu, F., Fiori, E., Rebora, N., Parodi, A., Mihalović, A., Ivković, M., Dekić, L., van Verseveld, W., Nuissier, O.,



- Ducrocq, V., D'Agostino, D., Galizia, A., Danovaro, E., & Clematis, A. (2015). Hydrometeorological multi-model ensemble simulations of the 4 November 2011 flash flood event in Genoa, Italy, in the framework of the DRIHM project. *Natural Hazards and Earth System Sciences*, 15(3), 537–555. <https://doi.org/10.5194/nhess-15-537-2015>
- Hersbach, H., Bell, B., Berrisford, P., Hirahara, S., Horányi, A., Muñoz-Sabater, J., & Thépaut, J. N. (2020). The ERA5 global reanalysis. *Quarterly Journal of the Royal Meteorological Society*, 146(730), 1999–2049. <https://doi.org/10.1002/qj.3803>
- Hingray, B., Bouvier, C., Desbordes, M., & Cappelaere, B. (2000). Inondations urbaines: un indicateur géométrique caractéristique du comportement hydraulique du bâti. *Revue des Sciences de l'Eau*, 13(1), 85–100.
- Hofmann, J., & Schüttrumpf, H. (2019). Risk-based early warning system for pluvial flash floods: Approaches and foundations. *Geosciences*, 9(3), 127. <https://doi.org/10.3390/geosciences9030127>
- Horn, F., & Elagib, N. A. (2018). Building socio-hydrological resilient cities against flash floods: Key challenges and a practical plan for arid regions. *Journal of Hydrology*, 564, 125–132. <https://doi.org/10.1016/j.jhydrol.2018.07.001>
- Huffman, G. J., Stocker, E. F., Bolvin, D. T., Nelkin, E. J., & Tan, J. (2019). GPM IMERG final precipitation L3 half hourly 0.1-degree x 0.1-degree V06, Greenbelt, MD, Goddard Earth Sciences Data and Information Services Center (GES DISC). <https://doi.org/10.5067/GPM/IMERG/3B-HH/06>
- Imhoff, R. O., Overeem, A., Brauer, C. C., Leijnse, H., Weerts, A. H., & Uijlenhoet, R. (2020). Rainfall nowcasting using commercial microwave links. *Geophysical Research Letters*, 47(19), e2020GL089365.
- Javelle, P., Braud, I., Saint-martin, C., Payrastré, O., Borga, M., Gourley, J., Zappa, M., Javelle, P., Braud, I., Saint-martin, C., Payrastré, O., & Gaume, E. (2016). Improving flash flood forecasting and warning capabilities. In *The Mediterranean region under climate change. A scientific update* (pp. 587–595). IRD Editions.
- Le Barbé, L., Lebel, T., & Tapsoba, D. (2002). Rainfall variability in West Africa during the years 1950–90. *Journal of Climate*, 15(2), 187–202.
- Lee, J. H., Yuk, G. M., Moon, H. T., & Moon, Y.-I. (2020). Integrated flood forecasting and warning system against flash rainfall in the small-scaled urban stream. *Atmosphere*, 11(9), 971. <https://doi.org/10.3390/ATMOS11090971>
- Lhomme, J., Bouvier, C., & Perrin, J. (2004). Applying a GIS-based geomorphological routing model in urban catchments. *Journal of Hydrology*, 299(3–4), 203–216. [https://doi.org/10.1016/S0022-1694\(04\)00367-1](https://doi.org/10.1016/S0022-1694(04)00367-1)
- Llort, X., Sánchez-Diezma, R., Rodríguez, Á., Sancho, D., Berenguer, M., & Sempere-Torres, D. (2014). Floodalert: A simplified radar-based EWS for urban flood warning. Proceedings of the 11th international conference on Hydroinformatics HIC.
- Lumbroso, D. (2018). How can policy makers in sub-Saharan Africa make early warning systems more effective? The case of Uganda. *International Journal of Disaster Risk Reduction*, 27, 530–540. <https://doi.org/10.1016/j.ijdr.2017.11.017>
- Lumbroso, D. (2020). Flood risk management in Africa. *Journal of Flood Risk Management*, 13(3), e12612. <https://doi.org/10.1111/jfr3.12612>
- Lumbroso, D., Rance, J., Pearce, G., & Wade, S. (2014). Final report: Science for humanitarian emergencies and resilience (SHEAR) scoping study. Evidence on demand: Climate, environment, infrastructure and livelihoods, commissioned by DFID (HR Wallingford). [https://doi.org/10.12774/eod\\_cr.june2014.lumbrosoetal](https://doi.org/10.12774/eod_cr.june2014.lumbrosoetal)
- Mahmood, M. I., Elagib, N. A., Horn, F., & Saad, S. A. G. (2017). Lessons learned from Khartoum flash flood impacts: An integrated assessment. *Science of the Total Environment*, 601–602, 1031–1045. <https://doi.org/10.1016/j.scitotenv.2017.05.260>
- Mathon, V., Laurent, H., & Lebel, T. (2002). Mesoscale convective system rainfall in the Sahel. *Journal of Applied Meteorology*, 41(11), 1081–1092. [https://doi.org/10.1175/1520-0450\(2002\)041<1081:MCSRIT>2.0.CO;2](https://doi.org/10.1175/1520-0450(2002)041<1081:MCSRIT>2.0.CO;2)
- Mukim, M. (2018). *Bamako urban sector review: An engine of growth and service delivery* (No. 127221). <http://documents1.worldbank.org/curated/en/154691549486819482/pdf/127221-repl-Bamako-Report-final-v4.pdf>
- Odume, N., & Slaughter, A. (2018). Africa needs to invest more in its water professionals. *The Conversation*. <https://theconversation.com/africa-needs-to-invest-more-in-its-water-professionals-91398>
- Panthou, G., Lebel, T., Vischel, T., Quantin, G., Sane, Y., Ba, A., & Diopkane, M. (2018). Rainfall intensification in tropical semi-arid regions: The Sahelian case. *Environmental Research Letters*, 13(6), 064013. <https://doi.org/10.1088/1748-9326/aac334>
- Pappenberger, F., Cloke, H. L., Parker, D. J., Wetterhall, F., Richardson, D. S., & Thielen, J. (2015). The monetary benefit of early flood warnings in Europe. *Environmental Science and Policy*, 51, 278–291. <https://doi.org/10.1016/j.envsci.2015.04.016>
- Pastorek, J., Fencel, M., Rieckermann, J., & Bareš, V. (2019). Commercial microwave links for urban drainage modelling: The effect of link characteristics and their position on runoff simulations. *Journal of Environmental Management*, 251, 109522. <https://doi.org/10.1016/j.jenvman.2019.109522>
- Perera, D., Agnihotri, J., Seidou, O., & Djalante, R. (2020). Identifying societal challenges in flood early warning systems. *International Journal of Disaster Risk Reduction*, 51, 101794. <https://doi.org/10.1016/j.ijdr.2020.101794>
- Perera, D., Seidou, O., Agnihotri, J., Rasmy, M., Smakhtin, V., Coulibaly, P., & Mehmood, H. (2019). Flood early warning systems: A review of benefits, challenges and prospects. UNU-INWEH Report Series, Issue 08. United Nations University Institute for Water, Environment and Health. <http://inweh.unu.edu/publications/>
- Rai, R. K., van den Homberg, M. J. C., Ghimire, P., & McQuistan, C. (2020). Cost-benefit analysis of flood early warning system in the Karnali River basin of Nepal. *International Journal of Disaster Risk Reduction*, 47, 101534. <https://doi.org/10.1016/j.ijdr.2020.101534>
- Republic of Mali. (2019). Evaluation rapide des Dommages, des Pertes et des Besoins post-inondation à Bamako (Rapid PDNA), Bamako. <https://www.gfdr.org/fr/publication/bamako-pdna>
- Republic of Mali. (2020). Elaboration et mise en oeuvre d'un programme d'éducation sur les risques climatiques et d'inondation au Mali. Rapport final. [https://pgrci-mali.org/wp-content/uploads/2020/01/Rapport-final\\_Programme-Education.pdf](https://pgrci-mali.org/wp-content/uploads/2020/01/Rapport-final_Programme-Education.pdf)
- Satgé, F., Defrance, D., Sultan, B., Bonnet, M. P., Seyler, F., Rouché, N., & Paturel, J. E. (2020). Evaluation of 23 gridded

- precipitation datasets across West Africa. *Journal of Hydrology*, 581, 124412. <https://doi.org/10.1016/j.jhydrol.2019.124412>
- Seidou, O., & Diab  t  , C. (2019). Mise en place d'un m  canisme op  rationnel de suivi et d'alerte pr  coce aux inondations au Mali. [https://pgrci-mali.org/wp-content/uploads/2019/12/RAPPORT\\_FINAL\\_SAP\\_MALI-.pdf](https://pgrci-mali.org/wp-content/uploads/2019/12/RAPPORT_FINAL_SAP_MALI-.pdf)
- SOMAGEF. (2019). Etude de la d  finition des indicateurs de vuln  rabilit  s et production des cartes des infrastructures situ  es dans les zones d'inondation du PGRCI. Rapport final. <https://pgrci-mali.org/wp-content/uploads/2019/12/Rapport-Final-d  finition-indicateurs-de-vuln  rabilit  -Cartographie-zone-inondablex.pdf>
- Taylor, C. M., Belusic, D., Guichard, F., Parker, D. J., Vischel, T., Bock, O., & Panthou, G. (2017). Frequency of extreme Sahelian storms tripled since 1982 in satellite observations. *Nature*, 544(7651), 475–478. <https://doi.org/10.1038/nature22069>
- Tazen, F., Diarra, A., Kabore, R. F. W., Ibrahim, B., Bologo/Traor  , M., Traor  , K., & Karambiri, H. (2018). Trends in flood events and their relationship to extreme rainfall in an urban area of Sahelian West Africa: The case study of Ouagadougou, Burkina Faso. *Journal of Flood Risk Management*, 12, e12612. <https://doi.org/10.1111/jfr3.12507>
- Tramblay, Y., Bouvier, C., Ayral, P. A., & Marchandise, A. (2011). Impact of rainfall spatial distribution on rainfall-runoff modeling efficiency and initial soil moisture conditions estimation. *Natural Hazards and Earth System Science*, 11(1), 157–170. <https://doi.org/10.5194/nhess-11-157-2011>
- Turko, M., Gosset, M., Kacou, M., Bouvier, C., Chahinian, N., Boone, A., & Alcoba, M. (2021). Rainfall measurement from commercial microwave links for urban hydrology in Africa: A simulation framework for sensitivity analysis. *Journal of Hydro-meteorology*, 22(7), 1819–1834. <https://doi.org/10.1175/JHM-D-20-0163.1>
- UN-ISDR. (2013). Global survey of early warning systems: An assessment of capacities, gaps and opportunities toward building a comprehensive global early warning system for all natural hazards. Platform for the promotion of early warning (UNISDR—PPEW). UN: P. 46. <http://www.unisdr.org/%0A2006/ppew/info-resources/ewc3/Global-Survey-of-Early-Warning-Systems.pdf>
- Verkade, J. S., & Werner, M. G. F. (2011). Estimating the benefits of single value and probability forecasting for flood warning. *Hydrology and Earth System Sciences*, 15(12), 3751–3765. <https://doi.org/10.5194/hess-15-3751-2011>
- Yang, T.-H., Yang, S.-C., Ho, J.-Y., Lin, G.-F., Hwang, G.-D., & Lee, C.-S. (2015). Flash flood warnings using the ensemble precipitation forecasting technique: A case study on forecasting floods in Taiwan caused by typhoons. *Journal of Hydrology*, 520, 367–378. <https://doi.org/10.1016/j.jhydrol.2014.11.028>

**How to cite this article:** Chahinian, N., Alcoba, M., Demb  l  , N. d. J., Cazenave, F., & Bouvier, C. (2022). Evaluation of an early flood warning system in Bamako (Mali): Lessons learned from the flood of May 2019. *Journal of Flood Risk Management*, e12878. <https://doi.org/10.1111/jfr3.12878>